vulcanhammer.info
August 2020

DOI: 10.13140/RG.2.2.10487.04002

OTC 5397 Revisited: Analysis of Cushioned Pile Hammers

Don C. Warrington, Ph.D., P.E.
University of Tennessee at Chattanooga
Department of Mechanical Engineering

Warrington (1987) was a detailed analysis of the mechanics of impact pile driving using semi-infinite pile theory and pile impedance concepts. In this paper a review and expansion of the basic concepts set forth in this paper is performed. First, a review of the basic concepts and equations set forth in the original is first performed with revised notation. From here a different numerical method is used to analyze the equations and a parametric study of the results is performed, giving an illustration of the resulting trends. Finally three test cases, one of which came from the original paper, are done to compare the results of the present model to specific situations.

Keywords: pile driving, pile impedance, offshore, pipe piles, hammer cushions

Introduction

For most practical problems of driven piles, the numerical, non-linear wave equation is used to either predict the performance of the hammer-pile-soil system during driving or inversely to estimate the static capacity of the pile from dynamic performance. Underpinning the use of these methods (especially inverse ones) is semi-infinite pile theory, which predicts the performance of the head of the pile during the impact of the hammer. In most cases, during the early stages of that impact, semi-infinite pile theory can predict the force-time and velocity-time performance of the pile head; the subsequent variation forms the basis of the interpretation of pile head instrumentation for the purpose of estimating static performance of the pile. Warrington (1997) discusses semi-infinite pile theory in detail.

The first comprehensive attempt to combine semi-infinite pile theory with pile impedance-matching–and thus using it as a possible predictor of pile performance during driving–was Parola (1970). Warrington (1987) continued with that analysis and extended it to impact hammers without a hammer cushion. This work also attempted to use the results of semi-infinite pile theory to estimate the static capacity of the pile, although the realities of wave theory and resistance characteristics of actual piles hindered the progress of the work.

Use of this did not end with Warrington (1987); Deeks and Randolph (1993) used an elegant closed-form solution to predict pile head performance during impact. Warrington (1997) also developed closed-form solutions for both pile head and general pile response to impact. In addition Take, Valsangkar, and Randolph (1999) extended the application of the theory to piles with pile cushions as well as hammer ones, making them more applicable to concrete piles.

The purpose of this paper is to revisit Warrington (1987) by taking the theory developed there, reconstructing the model (the original was lost) and analyzing the results more in the direction of hammer-pile interaction rather than attempting to develop a capacity prediction method. In doing this it was hoped that new insights could be made on the problem.

Basic Theory

The basic system under investigation is shown in Figure 1. In this study steel piles will be considered exclusively, since they are almost always driven without a pile cushion. Although pipe piles are featured, this is largely due to an emphasis on offshore piling, which because of its length more perfectly embodies this type of hammer-pile response. However, it is certainly possible to use this theory with H-piles and other steel shapes as well. The ram and ram point operate as a unit. The hammer cushion is modeled as an inextensible spring without dampening or friction. The ram and cap are modeled as rigid masses, and the pile as a velocity-dependent "dashpot" in accordance with semi-infinite pile theory.

Governing Equations

The system can be modeled using a system of two ordinary, second-order differential equations. The key to simplifying the solution and analysis of these equations, first posited by Parola (1970), is a change in the time variable as follows:

$$\tau = t\omega_0 \tag{1}$$

where

$$\omega_0 = \sqrt{\frac{k}{m_s}} \tag{2}$$

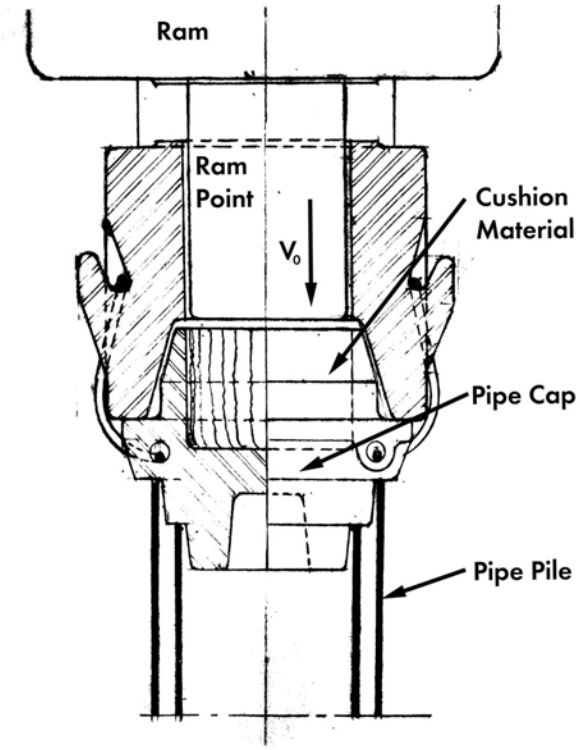

Figure 1. Hammer-Cap-Pile System

Neglecting the effect of gravity, the equations of motion can thus be rewritten

$$\frac{d^2}{d\tau^2}X_1(\tau) - X_2(\tau) + X_1(\tau) = 0 \tag{3}$$

$$\frac{\frac{d^2}{d\tau^2}X_2(\tau)}{m'} + z'\frac{d}{d\tau}X_2(\tau) + X_2(\tau) - X_1(\tau) = 0$$

where

$$z' = \frac{Z_p}{Z_s} \tag{4}$$

$$Z_p = \sqrt{\rho E A} \tag{5}$$

$$Z_s = \sqrt{m_s k} \tag{6}$$

and

$$m' = \frac{m_s}{m_c} \tag{7}$$

Both $X(\tau)$ variables in Equations 3 and their first and second derivatives have units of length. Once Equations 3 are solved the variables can be converted back to real displacements, velocities and accelerations as follows:

$$\begin{aligned} X_n(\tau) &= x_n(t) \\ \frac{d}{d\tau}X_n(\tau)\omega_0 &= \frac{d}{dt}x_n(t) \\ \frac{d^2}{d\tau^2}X_n(\tau)\omega_0^2 &= \frac{d^2}{dt^2}x_n(t) \end{aligned} \tag{8}$$

However, the significance of these variables is more easily seen if the case of the rigid base is considered.

Rigid Base Case

If a rigid base to the hammer cushion is assumed (or $Z_p \to \infty$) Equations 3 reduce to

$$\frac{d^2}{d\tau^2}X_1(\tau) + X_1(\tau) = 0 \tag{9}$$

In real time the initial conditions for this equation are $x_1(0) = X_1(0) = 0$ and $\frac{d}{dt}x(0) = V_0$. However, if we apply this last initial condition to Equation 8, we can express the initial velocity as follows:

$$\frac{d}{d\tau}X_1(0) = L_{sys} = \frac{V_0}{\omega_0} \tag{10}$$

The physical significance of the system length L_{sys} is that it represents the maximum compression of the hammer cushion for the condition of the rigid base. This variable, however, is the key to understanding the behavior of these equations and the system.

The solution of Equation 9 is

$$X_1(\tau) = L_{sys} sin(\tau) \tag{11}$$

The derivatives of this equation are trivial; the maximum deceleration of the ram in reduced variables is

$$\frac{d^2}{d\tau^2}X_1(\frac{\pi}{2}) = -L_{sys} \tag{12}$$

Solution of the Equations

Now we are in a position to solve Equations 3. Deeks and Randolph (1993) solved these in closed form; however, the complexities involved with actually implementing this made a numerical solution inviting, as was the case for Warrington (1987). That effort used a fourth-order Runge-Kutta method; in this case a Newmark method, as described by Hughes (2000), was employed. The best place to start is the recursion equation, which is

$$Aa_{n+1} = F_{n+1} - C\left(v_n + (1-\gamma)\Delta t a_n\right) - K\left(d_n + \Delta t v_n + \frac{\Delta t^2(1-2\beta)}{2}a_n\right) \tag{13}$$

where

$$A = M + \gamma \Delta t C + \beta \Delta t^2 K \tag{14}$$

This matrix can be constructed from Equations 3 by noting that (James, Smith, Wolford, and Whaley (1989))

$$M = \begin{bmatrix} 1 & 0 \\ 0 & m'^{-1} \end{bmatrix} \tag{15}$$

$$C = \begin{bmatrix} 0 & 0 \\ 0 & z' \end{bmatrix} \tag{16}$$

$$K = \begin{bmatrix} 1 & -1 \\ -1 & 1 \end{bmatrix} \tag{17}$$

The symmetric 2×2 matrix A is easily assembled. For many problems inverting this matrix is impractical; in this case it is simple, and the acceleration at the end of the time step is simply

$$a_{n+1} = A^{-1}\left(F_{n+1} - C\left(v_n + (1-\gamma)\,\Delta t a_n\right) - K\left(d_n + \Delta t v_n + \frac{\Delta t^2\,(1-2\beta)}{2} a_n\right)\right) \tag{18}$$

The displacements and velocities (in vector form) can then be computed as follows:

$$d_{n+1} = d_n + \Delta t v_n + \Delta t^2 \left(\left(\frac{1}{2} - \beta\right) a_n + \beta a_{n+1}\right) \tag{19}$$

$$v_{n+1} = v_n + \Delta t\left((1-\gamma)\,a_n + \gamma a_{n+1}\right) \tag{20}$$

The use of a, v and d do not mean that it is necessary to use the actual (as opposed to the reduced) variables; they only mean that the method requires them to be put in vector form. The external force vector F is null at all times.

The initial condition vector d_0 is null. The vector v_0 for the initial velocities and Equations 3 is given as

$$v_0 = \begin{bmatrix} L_{sys} \\ 0 \end{bmatrix} \tag{21}$$

Because of the simplicity of the matrices and vectors, it is possible to compute the acceleration, velocity and displacement at the end of the time steps in one step for each rather than having to go through a predictor-corrector process as is customary with Newmark's Method. The method has several options for explicit or implicit solution (and the time step necessary that goes with each one) depending upon the values of γ and β. In this case, in order to obtain meaningful acceleration-, velocity- and displacement-time histories, and to "switch equations" due to the inextensibility of the hammer cushion, the time step was small, and the use of an implicit method had little advantage.

Considering the inextensibility of the hammer cushion, the only change in the method necessary when tension was detected in the hammer cushion was to switch the stiffness matrix in Equation 17 to the null matrix. The program monitored the relative positions of the ram and cap and was capable of alternating this stiffness matrix during the analysis. The method was implemented in a FORTRAN 77 program and the code for Equations 18, 19 20 was done by employing Maple V Release 3 to construct the matrices, perform the necessary inversion and generate the code. These are old tools but in this case they are effective and economical.

Since Equations 3 represent a linear transformation and the only input is Equation 21, the results are a scalar multiple of L_{sys} (Gelfand (1961).) This made is possible to both analyze specific cases and perform parametric studies by assuming $L_{sys} = 1$. Although this simple proportionality may not hold past the point where the system becomes inextensible, most of the peak quantities take place when the ram, cushion and cap are all in contact with each other; the only one that frequently does not is the time for stopping the analysis, which is based on the velocity of the cap nearing zero.

Parametric Study

The most broad-based application of the routine was the parametric study. Here $L_{sys} = 1$ and the two ratios were varied within a range of $0.1 \leq z' \leq 1.6$ and $1 \leq m' \leq 10$, as was the case with Warrington (1987). The various parameters and a discussion of the results of each follows.

Ram and Cap Acceleration

The peak ram deceleration and the peak cap acceleration are shown in Figures 2 and 3 respectively. The two results are almost mirror images of each other. The ram deceleration tends to be the greatest when m' is the lowest and z' is the highest, and the cap acceleration trends in the opposite direction. Put another way, one would expect lighter caps (relative to the ram mass or weight) to not load the ram as severely during impact and at the same time experience higher loads themselves. One other major difference is that the cap acceleration tends to be greater than the ram deceleration, which would indicate that, all other things being equal, cap life would be expected to be shorter than the hammer in general and the ram in particular.

Ram Exit Velocity and Rebound Energy

The next two results are basically the same as each other but expressed differently. They are not peak values but "exit" values of ram velocity and kinetic energy after separation from the cushion material and cap. Figures 4 and 5 show the ram velocity and proportion of the energy to the total kinetic energy of the ram at impact. Although velocity varies widely across the spectrum of impedance ratios, the fact that the rebound energy is the square of the velocity makes the significance of the lower rebound velocities clear. Rebound

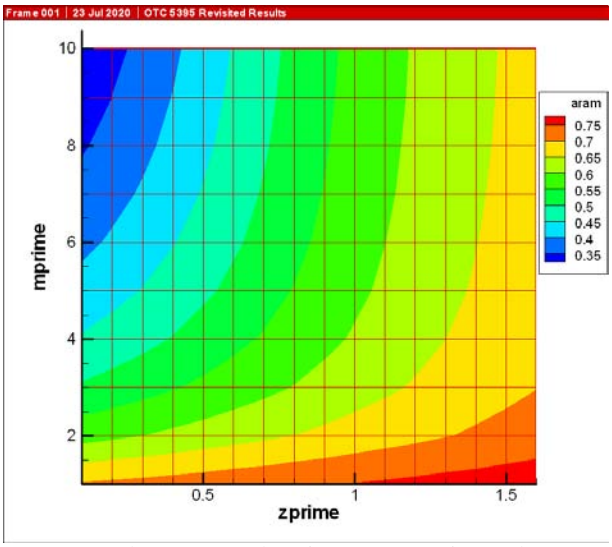

Figure 2. Peak Ram Acceleration, Parametric Study

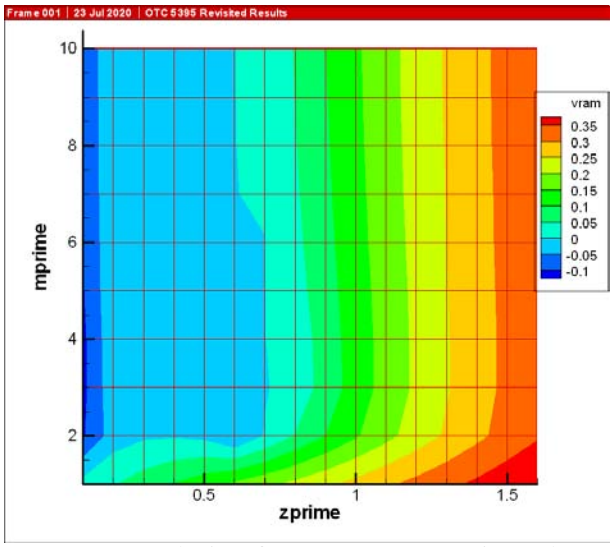

Figure 4. Ram Velocity after Impact, Parametric Study

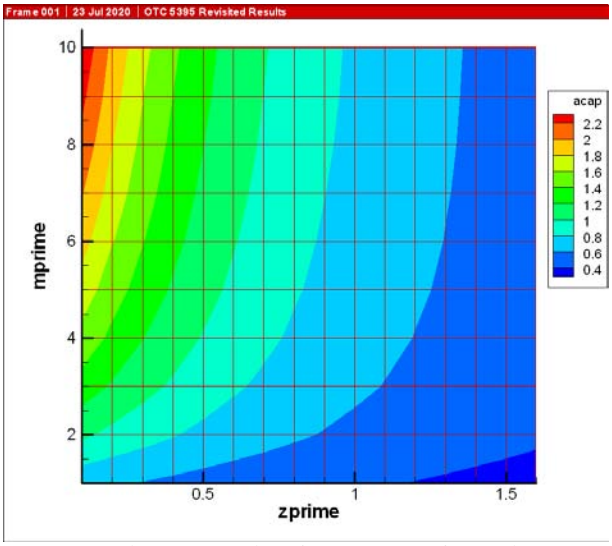

Figure 3. Peak Cap Acceleration, Parametric Study

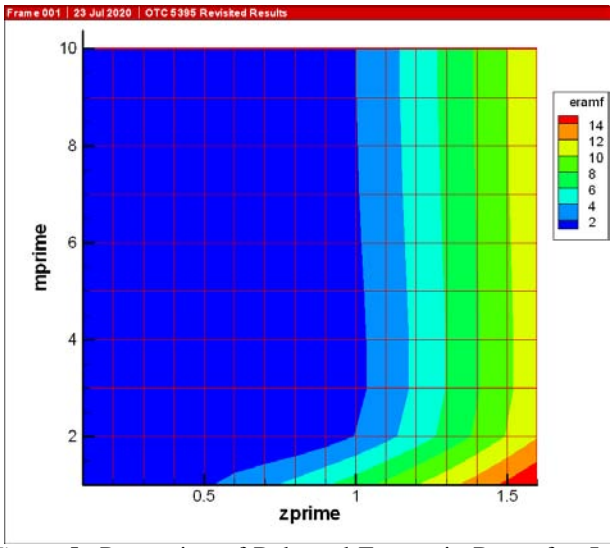

Figure 5. Proportion of Rebound Energy in Ram after Impact, percent, Parametric Study

in pile driving is generally associated with the return of elastic pile and soil energy to the hammer. However, Figure 5 in particular shows that, for high impedance piles, rebound can take place before the energy even gets into the pile, and that very high impedance ratios should probably be avoided.

It is also noteworthy that the trend of the results changes significantly for values of $m' \geq 2$. For values in this range, the rebound proportion is largely independent of m'. This "knee" in the results will be evident elsewhere. The use of caps with $m' \leq 2$ is uncommon and thus this part of the analysis can be neglected.

Cap Velocity

The peak cap velocity is shown in Figure 6. The peak cap velocity is an important parameter in that the peak pile head force is the product of it and the pile impedance. For values of $m' \geq 2$, the peak cap velocity is for the most part a function of the impedance ratio. Lower impedance piles can result in very high cap velocities; in practice this is an unstable condition and safety concerns can arise. Low-impedance piles are generally not efficient in their transfer of energy to the soil.

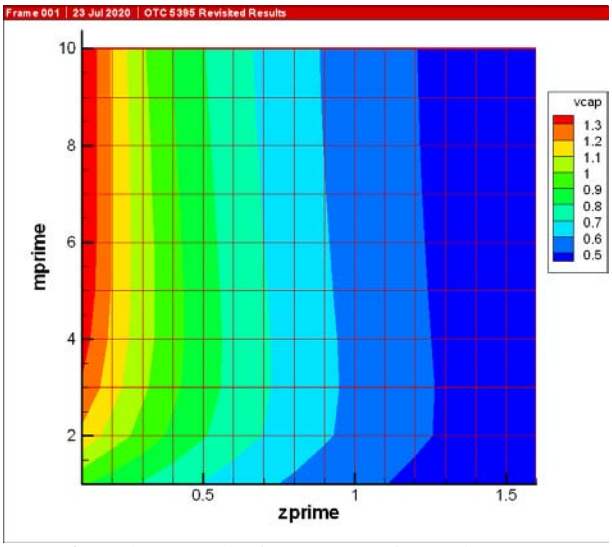

Figure 6. Peak Cap Velocity, Parametric Study

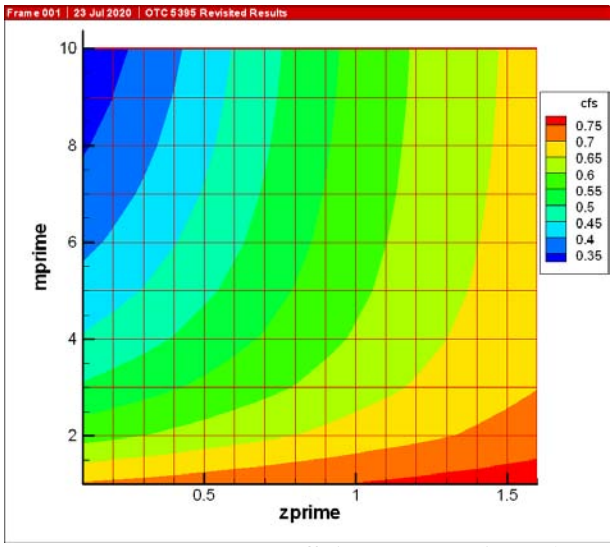

Figure 7. Hammer Force Coefficient, Parametric Study

Force Coefficients

The force coefficient is the ratio of an actual peak force to the maximum ram force with a rigid base. There are actually two of them in this system. The first is the ram force coefficient, which is

$$C_{fs} = \frac{\frac{d^2}{d\tau^2} X_1(\tau)_{max}}{L_{sys}} \tag{22}$$

The second is the pile force coefficient, and this is

$$C_{fp} = \frac{| \frac{d}{d\tau} X_2(\tau) |_{max}}{L_{sys}} \tag{23}$$

The values for each of these coefficients appears in Figures 7 and 8. The hammer force coefficient is generally higher than its pile counterpart, as one would expect. It is also more dependent upon m' as well; heavier caps tend to raise the hammer force, which is related to its deceleration (see Figure 2.) The pile force coefficient is mostly dependent upon z', and rises with increasing pile impedance.

Run Time and Pile Head Displacement

For rigid base cases, it is evident from Equation 11 that the ram force returns to zero at $\tau = \pi$. When the base is not rigid, the answer is not so clear. The program was set up so that, within a tolerance, the program would stop when the pile head velocity reached zero. Figure 9 shows the run times for these in radians. Longer run times are associated with lower pile impedances.

This is also related to the last parameter, the final pile head displacement, shown in Figure 10. The results are fairly consistent until low pile impedances are encountered, at which point large displacements take place. This result

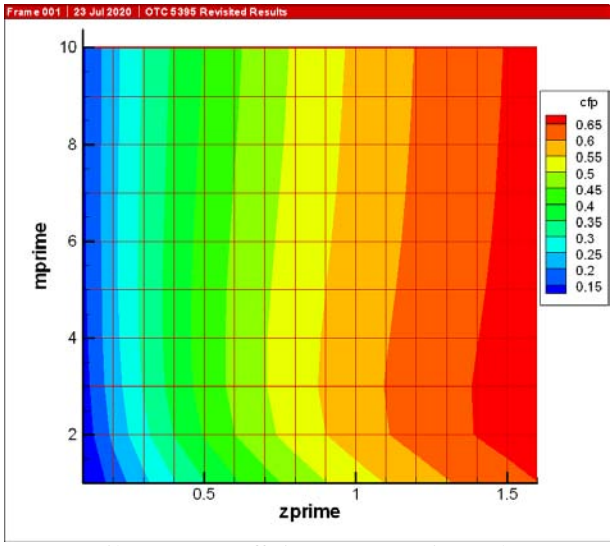

Figure 8. Pile Force Coefficient, Parametric Study

complements the result of the pile head velocity; low pile impedances result in large pile head movement and high cap velocities even before the rest of the pile moves.

Case Histories

With the parametric study complete, some case histories are in order. Each of these case histories uses a different method to arrive at the results, which makes comparison interesting. It is also possible to see some aspects of the algorithm viewed in more detail than is possible with the parametric study.

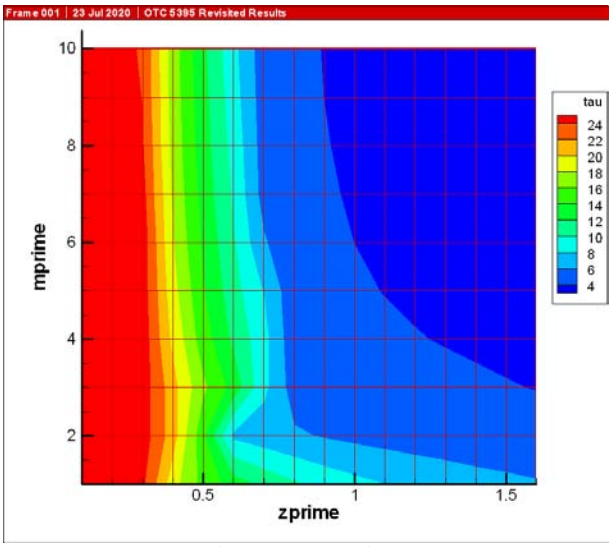

Figure 9. Total Run Time, Parametric Study

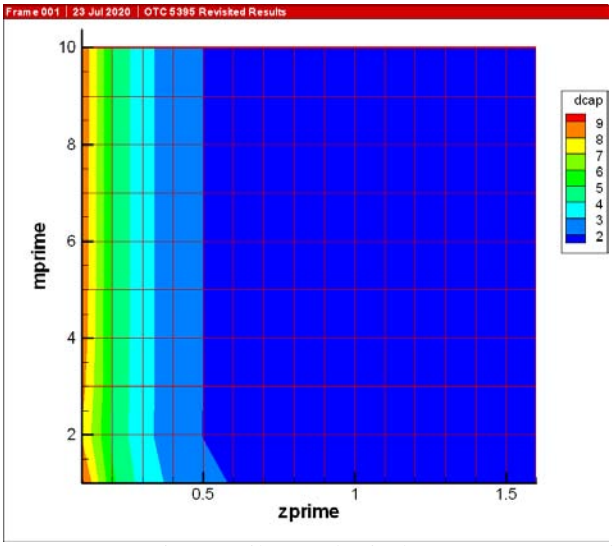

Figure 10. Maximum Pile Head Displacement, Parametric Study

Table 1
Basic Parameters for Warrington (1987) Test Case

Rated Striking Energy, ft-lbs	312500
Weight of Striking Parts, lbs.	62500
Cap Weight, lbs.	32055
Equivalent Stroke, ft.	5
Efficiency, percent	75
Net Striking Energy, ft-lbs	234375
Impact Velocity of Ram, ft/sec	15.53
Cushion Stiffness, kips/ft	306796.2
Ram Frequency, rad/sec	397.41
Maximum Theoretical Ram Deceleration, g's	191.87
Ideal Impact Force, kips	5996.1
Hammer Impedance, lb-sec/ft	771992.6
Ram-Cap Mass Ratio	1.95
System Length, in.	0.469

Warrington (1987)

The first case history is taken from Warrington (1987). It concerns a Vulcan 560; the parameters relevant to this project are shown in Table 1. The original paper treated this problem parametrically in that it varied the value of z'; thus, four cases were chosen using different impedance ratios (and by extension pile cross-sectional areas.) The results for these cases are shown in Table 2. Within numerical method variations, the results shown in Table 2 are the same (including maximum cap velocity and pile head stress) as with the original monograph with one notable exception: pile head force. As the original analysis results and background information are lost, it is impossible to determine the reason for this discrepancy.

Table 2 also shows the changes in results with variations in z'. These results agree with the results of the parametric study above, but place them in a more physically realistic context. Further understanding of this context can be found in the time plots for the four impedance ratios, which are given in Figures 11, 12, 13 and 14. The plots include the reduced acceleration, velocity and displacement for both ram and cap (the displacements are actual numbers.) The following can be noted about these plots:

- With both the ram and cap accelerations, it is easy to see the discontinuity caused by the inextensibility of the cushion and the separation of the ram from the cushion and cap.
- With the lower impedance piles, we can also see that the ram and cushion re-establish contact after initial separation; in the case of $z' = 0.2$ this takes place twice. Although this imparts further energy to the cap and thus the pile, it also shows a "chattering" taking place in the initial impact phase, which underscores the instability taking place during the impact on low-impedance piles. The large pile head displacements from impact can also be noted with the low-impedance cases.
- The peak cap velocity–and thus the peak pile head force–always takes place within the time of the initial impact of the ram on the cushion, although with the low impedance piles this is nearly not the case.
- The loss of the background material for the original study also means that time plot comparisons are not possible with this case history.

Warrington (1997)

This case compares the results of a true closed-form solution of the pile head response, which was then used in a closed-form solution of the wave equation for piles. The con-

Table 2
Results for Various Impedance Ratios

Result	$z' = 0.2$	$z' = 0.5$	$z' = 1$	$z' = 1.5$
Pile Cross-Sectional Area, in²	88.56	221.41	442.82	664.22
Pile Impedance, kip-sec/ft	154.3	385.8	771.7	1157.5
Maximum Ram Acceleration, g	114.16	119.86	129.16	137.55
Maximum Cap Acceleration, g	179.71	143.39	106.54	84.30
Maximum Cap Velocity, ft/sec	16.33	12.52	8.92	6.90
Maximum Pile Head Force, kips	2520.4	4829.9	6885.3	7990.5
Maximum Pile Head Stress, psi	28459.	21815.	15549.	12030.
Percentage Energy Returned to Ram	0.04	0.09	2.15	10.19

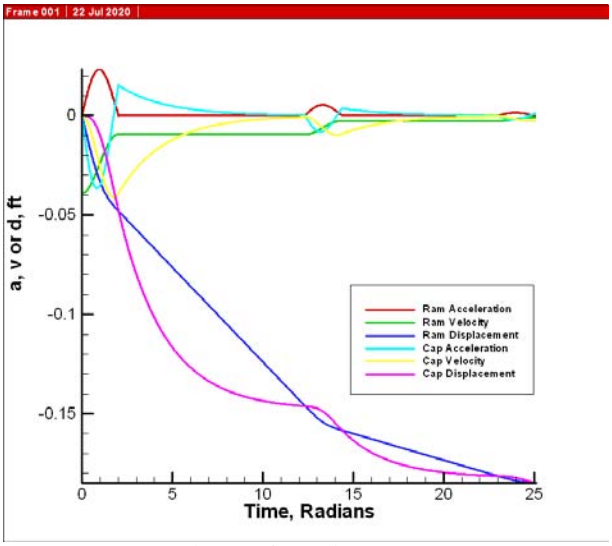

Figure 11. Ram and Cap Time Plots, $z' = 0.2$

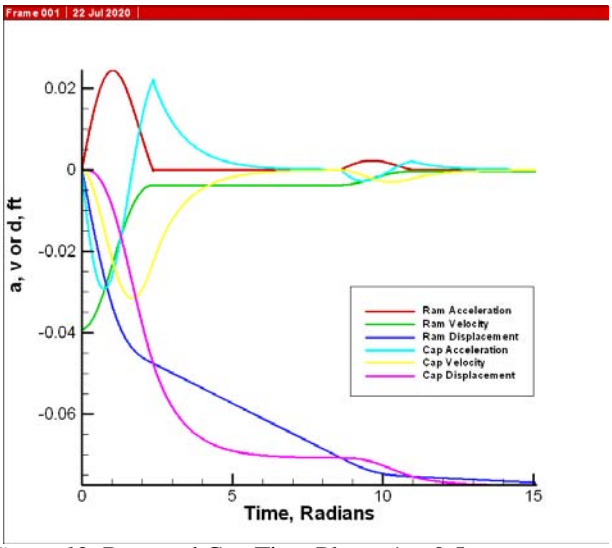

Figure 12. Ram and Cap Time Plots, $z' = 0.5$

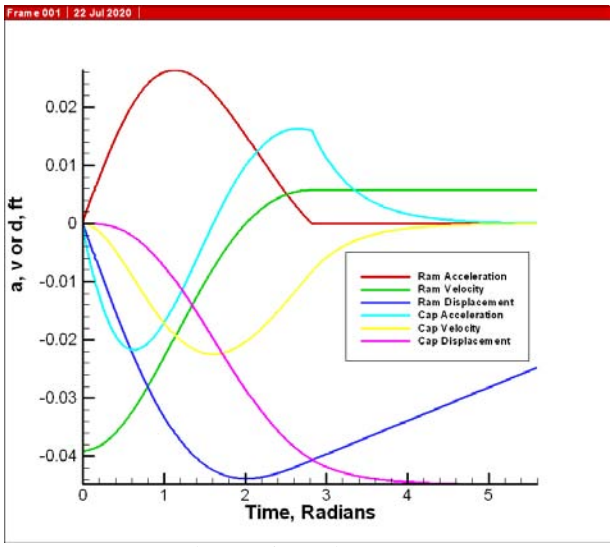

Figure 13. Ram and Cap Time Plots, $z' = 1.0$

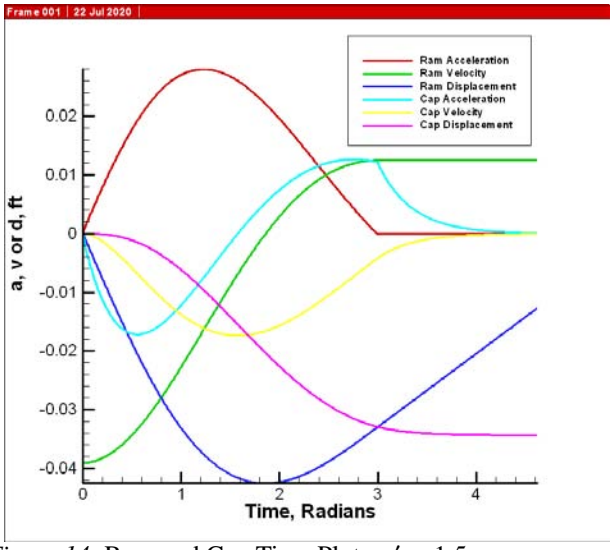

Figure 14. Ram and Cap Time Plots, $z' = 1.5$

figuration of the system is shown in Table 3. The hammer is a notional hammer in the range of a Vulcan 530.

As with the previous case, the values matched the original ones within numerical method accuracy. A simpler way to show this is to consider Figure 15, which shows a comparison between the pile head force of the original closed-form solution and one developed by the current model. The results are very close; the largest difference is towards the end, where the closed-form solution does not replicate the inextensibility of the cushion. The full time results of the current model are shown in Figure 16, where the break due to cushion extensibility can be seen.

Table 3
Basic Parameters and Results for Warrington (1997) Test Case

Rated Striking Energy, kJ	220.65
Mass of Striking Parts, kg	15000.
Cap Mass, kg	3000.
Equivalent Stroke, m	1.5
Efficiency, percent	80.
Net Striking Energy, kJ	176.52
Impact Velocity of Ram, m/sec	4.85
Cushion Stiffness, GN/m	2.45
Ram Frequency, rad/sec	404.14
Maximum Theoretical Ram Deceleration	199.93
Ideal Impact Force, MN	29.41
Hammer Impedance, MN-sec/m	6.062
Pile Cross-Sectional Area, m²	0.12064
Pile Impedance, MN-sec/m	4.88
Impedance Ratio	0.805
Ram-Cap Mass Ratio	5.
System Length, mm	12.
Maximum Ram Acceleration, g	110.59
Maximum Cap Acceleration, g	162.52
Maximum Cap Velocity, m/sec	3.16
Maximum Pile Head Force, MN	15.45
Maximum Pile Head Stress, MPa	128.04
Percentage Energy Returned to Ram	0.101

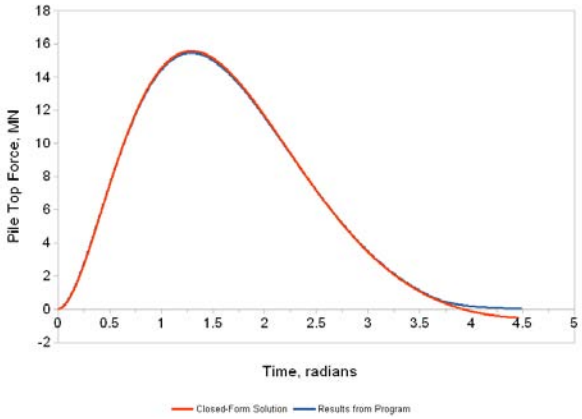

Figure 15. Ram Force Comparison Plot

Warrington (2016)

The last test case compares the program with the finite element program STADYN. The case involves the use of a Vulcan 5110 hammer driving long (150 m) offshore piling; with this length, it is assumed that the pile head force-time history would be developed before the pile actually moved relative to the soil. As with the previous case the input and output of the program is shown in Table 4.

In the original study the peak pile head force was 22.16 MN; GRLWEAP, which was also used to analyze the case, returned a value of 21.86 MN. Likewise, STADYN showed a maximum pile head velocity of 2.59 m/sec and GRLWEAP 2.48 m/sec. All velocities can be converted to reduced velocities by dividing the actual velocity by the ram frequency ω_0, and this was done for the ram and cap velocities for both STADYN and the current program. The results are shown in Figure 17. The comparison is interesting because it illustrates the different way each routine analyzes the problem.

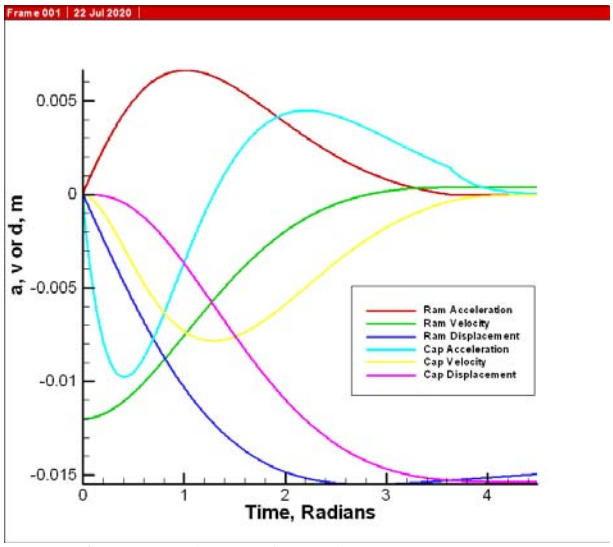

Figure 16. Ram and Cap Time Plots

With the reduced ram velocity, the trend for both is the same but STADYN's results "wander" around the current program. Although STADYN certainly experienced parasite oscillations, and some of the variation comes from these, another explanation is that, unlike the current program, STADYN does not model the ram as a rigid mass but as a rod divided up into axisymmetric elements, as can be seen in Figure 18. Stress waves travel within the rod, creating an oscillation within the ram that is reflected in the ram point force-time history.

Turning to the reduced cap velocity, the peak force from both STADYN and the program are very close; however, the STADYN results are "time shifted" slightly behind the current program. Although dispersive effects cannot be completely discounted (but see Warrington (2020),) another explanation can be seen in Figure 18 in that the cap, rather than being rigid, is also divided up into elements with distributed mass and elasticity. Additionally considering that the ram/cushion outside diameter is less than 60% of the pile outside diameter (see Figure 18,) it is possible that "beam effects" (or perhaps better "plate effects") in the cap are making the system more flexible and by doing so are causing the time shifting phenomenon that is observed. Although including the flexibility of the ram is routine in wave equation

Table 4
Basic Parameters and Results for Warrington (2016) Test Case

Rated Striking Energy, kJ	745.71
Mass of Striking Parts, kg	49896.
Cap Mass, kg	17872.
Equivalent Stroke, m	1.524
Efficiency, percent	67.
Net Striking Energy, kJ	499.63
Impact Velocity of Ram, m/sec	4.48
Cushion Stiffness, GN/m	1.516
Ram Frequency, rad/sec	174.31
Maximum Theoretical Ram Deceleration	79.54
Ideal Impact Force, MN	38.92
Hammer Impedance, MN-sec/m	8.697
Pile Cross-Sectional Area, m²	0.21165
Pile Impedance, MN-sec/m	8.566
Impedance Ratio	0.984
Ram-Cap Mass Ratio	2.79
System Length, mm	25.7
Maximum Ram Acceleration, g	50.42
Maximum Cap Acceleration, g	49.63
Maximum Cap Velocity, m/sec	2.62
Maximum Pile Head Force, MN	22.45
Maximum Pile Head Stress, MPa	106.09
Percentage Energy Returned to Ram	0.58

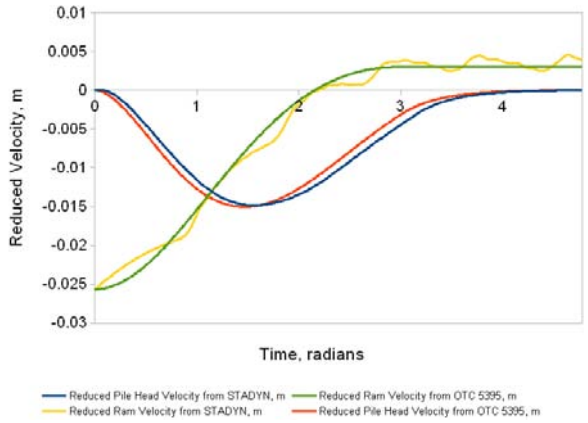

Figure 17. Reduced Velocity Comparison Plot

analyses, doing so for the cap–and taking into account these effects–is not.

The time plots for the ram and cap are shown in Figure 19.

Conclusions

1. The method presented here is a simple way to compute the initial loads and stresses on piles and hammers during impact. It is especially useful for long steel piles such as are common with offshore installations of all kinds, but can be

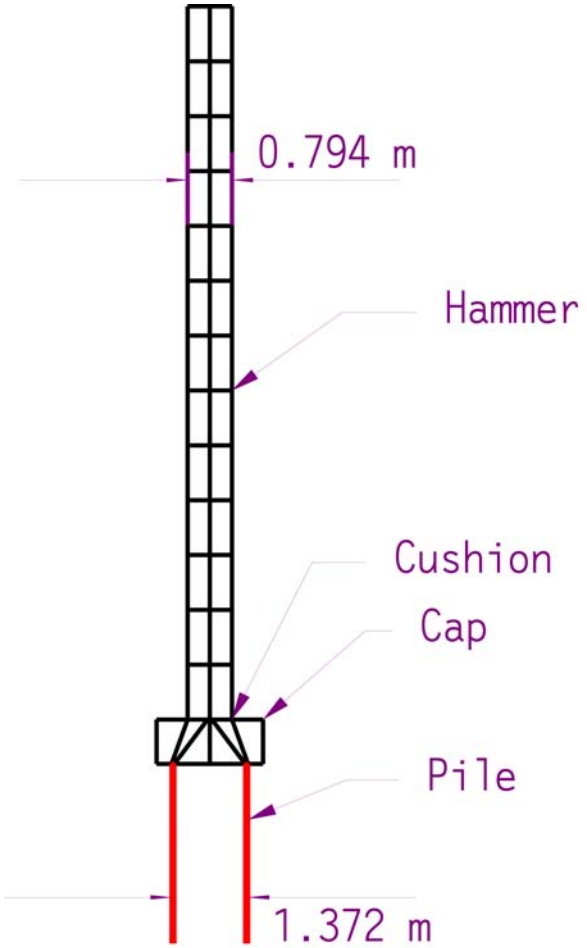

Figure 18. STADYN Axisymmetric Model for Ram, Cap and Pile Top

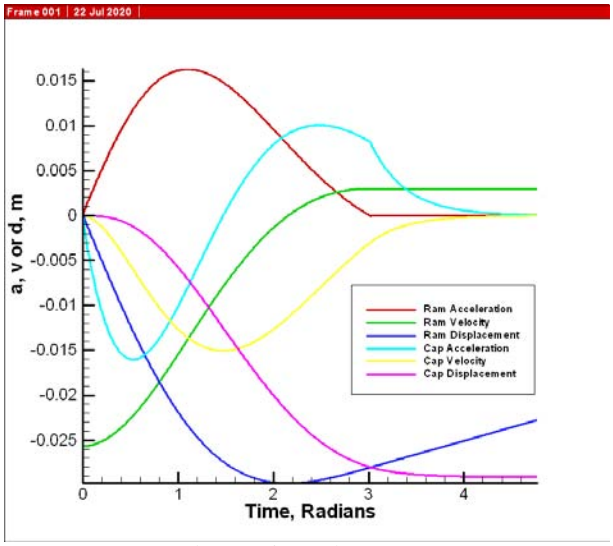

Figure 19. Ram and Cap Time Plots

applied to onshore piles as well.

2. The relationship of ram and cap weight is primarily dependent upon the desired distribution of the high absolute accelerations between the ram and the cap. Lighter caps tend to "put less load" on the ram, but if a cap is too light it will be more readily overstressed.

3. Generalizations of the results of this theory are difficult, and depend upon the ultimate objective of the specific project, but as a rule of thumb the optimum range of impedance ratios is around $0.5 \leq z' \leq 1$. Low impedance ratios lead to excessive pile head deflections and raising the impedance ratio past unity causes more of the ram's energy to be returned to it without movement of the pile.

4. "Beam effect" in large pipe caps can be significant but this effect has not been extensively studied.

Nomenclature

β	Newmark coefficient
Δt	Time step, radians
ω_0	Ram-cushion natural frequency, rad/sec
ρ	Density of pile material, $\frac{kg}{m^3}$ or $\frac{slugs}{ft^3}$
τ	Dimensionless time, radians
A	Newmark dynamic stiffness matrix
A	Pile cross-sectional area, m^2 or ft^2
a	Reduced acceleration vector, m
C	Damping matrix
C_{fp}	Pile force coefficient
C_{fs}	Ram force coefficient
d	Reduced displacement vector, m
F	External force vector, N or lbs
K	Stiffness matrix
k	Cushion Stiffness, N/m or lb/ft
L_{sys}	System length, m or ft
m'	Cap-Ram mass or weight ratio
m_s	Ram mass, kg or slugs
n or $n+1$	Subscripts in Newmark's Method for current or future time steps respectively, $n = 0$ is at initial time
t	Actual time, seconds
v	Reduced velocity vector, m
V_0	Impact velocity of ram, m/sec or ft/sec
$x(t)$	Actual displacement of ram (subscript $n = 1$) or cap (subscript $n = 2$), m or ft
$X_n(\tau)$	Reduced displacement of ram (subscript $n = 1$) or cap (subscript $n = 2$), m or ft
z'	Impedance Ratio
Z_p	Pile impedance, N-sec/m or lb-sec/ft
Z_s	Hammer impedance, N-sec/m or lb-sec/ft

References

Deeks, A. J., & Randolph, M. (1993, May). Analytical modelling of hammer impact for pile driving. *International Journal for Numerical and Analytical Methods in Geomechanics*, *17*, 279–302. doi: 10.1002/nag.1610170502

Gelfand, I. M. (1961). *Lectures on linear algebra* (No. 9). New York, NY: Interscience Publishers, Inc.

Hughes, T. J. (2000). *The finite element method*. Mineola, NY: Dover Publications, Inc.

James, M., Smith, G., Wolford, J., & Whaley, P. (1989). *Vibration of mechanical and structural systems*. New York, NY: Harper and Row.

Parola, J. F. (1970). *Mechanics of impact pile driving* (Unpublished doctoral dissertation). University of Illinois at Urbana-Champaign.

Take, W., Valsangkar, A., & Randolph, M. (1999, September). Analytical solution for pile hammer impact. *Computers and Geotechnics*, *25*(2), 57–74. doi: 10.1016/S0266-352X(99)00018-X

Warrington, D. C. (1987, April). A proposal for a simplified model for the determination of dynamic loads and stresses during pile driving. *Proceedings of the Offshore Technology Conference*, 329–338. doi: 10.4043/5395-MS

Warrington, D. C. (1997). *Closed form solution of the wave equation for piles* (Unpublished master's thesis). University of Tennessee at Chattanooga, Chattanooga, TN.

Warrington, D. C. (2016). *Improved methods for forward and inverse solution of the wave equation for piles* (Unpublished doctoral dissertation). University of Tennessee at Chattanooga, Chattanooga, TN.

Warrington, D. C. (2020, April). Inverse analysis of driven pile capacity in sands. *RESEARCH Dialogues Conference proceedings*. doi: 10.13140/RG.2.2.18499.14884